Decomposition of metal alkylamides, alkyls and halides at reducible oxide surfaces: mechanism of 'clean-up' during atomic layer deposition of dielectrics onto III-V substrates

*Sylwia Klejna, Simon D. Elliott**

Tyndall National Institute,

University College Cork,

Dyke Parade, Cork, Ireland

ABSTRACT: The pairing of high-*k* dielectric materials with high electron mobility semiconductors for transistors is facilitated when atomic layer deposition (ALD) is used to deposit the dielectric film. An interfacial cleaning mechanism ('clean-up') that results in consumption of semiconductor native oxides and in practically sharp dielectric/semiconductor interfaces has been observed during ALD of Al_2O_3, HfO_2, TiO_2 and Ta_2O_5 with various degrees of success. We undertake a comprehensive study using density functional theory (DFT) to explain differences in the performance of various classes of precursor chemicals in removing native oxide from III-V substrates. The study covers the metals Ta(V), Ti(IV), Zr(IV), Hf(IV), Al(III), Mg(II) combined with methyl, amide and chloride ligands. Of these, we show that clean-up is most effective when depositing MgO. Clean-up with metal alkylamides has a similar mechanism to clean-up with metal methyls insofar as oxygen is scavenged by the metal. The difference in operation of alkylamide and methyl ligands lies in the affinity of the ligand to the substrate. Alkylamide is shown to be prone to decomposition rather than the migration of the entire ligand evinced by methyl. We investigate the multi-step chemical processes associated with decomposition of alkylamide. These processes can also occur during later cycles of high-*k* ALD and give a chemical vapor deposition (CVD) component to the ALD process. These transformations lead to formation of clean-up products such as aziridine, ethene, N-methyl methyleneimine, hydrogen cyanide and methane. Some – but not all – of the reactions lead to reduction of surface As_2O_3 (*i.e.* clean-up). These results explain the experimentally-observed accumulation of metallic arsenic and arsenic suboxide at the interface. Such understanding can help achieve control of oxide-semiconductor interfaces through the appropriate choice of chemical precursor.

KEYWORDS atomic layer deposition (ALD), high-*k* dielectrics, III-V substrate, reducible oxide, clean-up effect, ALD precursor, metal alkylamide, ligand decomposition, density functional theory (DFT)

1. Introduction

The extensive research on pairing of high-*k* dielectrics materials with high electron mobility semiconductors has renewed interest in replacing SiO_2/Si based transistors for future generations of nanoelectronic devices. The key issue in combining high-*k* materials for the gate, such as Al_2O_3 and HfO_2, with GaAs or InGaAs III-V semiconductors for the channel is finding a stable passivation of the interface with acceptably low density of interface states. Several reports suggest that this can be partially achieved during deposition of the dielectric film using atomic layer deposition (ALD) [1]. The early stages of ALD growth determine the interface properties and therefore careful optimization of deposition conditions helps with improving device performance. An interfacial cleaning mechanism that results in consumption of semiconductor native oxides and in practically sharp dielectric/semiconductor interfaces has been observed during ALD of Al_2O_3 [2], HfO_2 [3], TiO_2 [4] and Ta_2O_5 [5] on GaAs and InGaAs. This has been called 'clean-up' or 'self-cleaning'. Although removing native oxides is not sufficient to solve the Fermi-level pinning problem in devices [6], it is an important step in the preparation of abrupt interfaces. The electrical characteristic of the device is improved though when appropriate and optimised passivation and ALD processing is enabled as suggested in [7].

While the phenomenon of native oxide thinning during semiconductor exposure to ALD metal precursors has been confirmed in several experiments, the chemistry of this process is not well understood. First reports on the clean-up effect documented an effective passivation of GaAs-based substrates with trimethylaluminium (TMA or $AlMe_3$; where Me = CH_3) when depositing Al_2O_3 [8]. For HfO_2 ALD, the clean-up effect was observed mainly when using hafnium alkylamides, with similar behaviour shown by tetrakis(ethylmethylamido)hafnium (TEMAH or $Hf(NEtMe)_4$; where Et = C_2H_5) or tetrakis(dimethylamido)hafnium (TDMAH, $Hf(NMe_2)_4$) [3a, 8-9]. A recent study shows that ALD processes utilizing alkylamide precursors featuring Ti (tetrakis(dimethylamido)titanium, TDMAT, $Ti(NMe_2)_4$) or Ta (pentakis(dimethylamido)tantalum, PDMAT, $Ta(NMe_2)_5$) also result in the same interfacial cleaning effect while depositing TiO_2 or Ta_2O_5 respectively [4b, 5]. These observations indicate that the common

requirement for self-cleaning is the use of organometallic or metalorganic precursors. However, the examples of the purely inorganic $HfCl_4$ and $TiCl_4$ ALD processes contradict this assumption. 'Clean-up' is also observed with the use of these precursors by Delabie *et al.* [3b] and Granados-Alpizar and Muscat [4a] but was not reported by Frank *et al.* [10].

Common experimental observations are found for interfacial cleaning with TMA and alkylamide precursors. Generally arsenic oxides are easier to remove than gallium oxides. Higher oxidation states of both As (As^{5+}) and Ga (Ga^{3+}) are more sensitive to reduction. Accumulation of metallic arsenic – arsenic suboxide at the interface has been observed for TMA based ALD [6a] and alkylamide based ALD [9]. It seems that elevating the temperature of the process significantly enhances the clean-up abilities of alkylamides, and this differentiates these processes from TMA-based clean-up [5, 11]. Granados-Alpizar and Muscat show differences in surface reactions during GaAs exposure to TMA and $TiCl_4$ pulses [4a]: both precursors remove the native oxide layer, but the mechanisms underlying this process seem to be fundamentally different. TMA deposits an Al_2O_3 layer and removes a portion of As from the surface, whereas $TiCl_4$ removes O and leaves the surface passivated with Cl atoms. The mechanism for removing oxides with the use of $HfCl_4$ differs also from the one for $TiCl_4$. The growth of hafnium oxide is enhanced [3b] and growth of titanium oxide is inhibited [4a]. These extensive and sometimes conflicting studies on interfacial self-cleaning show how little is understood about the chemistry occurring in the initial cycles of deposition of dielectrics.

In this study with the use of DFT we try to provide improved understanding of the chemical principles underlying 'clean-up' and thus rationalize experimental observations. There are not many studies available on mechanisms during early stages of growth on III-V semiconductors. Typical mechanisms occurring during ALD on other semiconductors (Si, Ge) are described in numerous publications, as reviewed by Elliott [12]. Previous atomic-scale simulations of clean-up mechanisms focused on the interaction of TMA with GaAs [13] and III-V native oxides [14]. TMA was shown to be able to reduce arsenic oxides into gaseous As_4 and solid GaAs, with Al_2O_3 formation and C lost as C_2H_6 [14]. DFT

revealed that the mechanistic step of reduction takes place when the CH_3 ligand migrates from surface-bound Al/As/Ga to O and gets oxidised, simultaneously reducing the III-V native oxide substrate. From the TMA example two interesting conclusions emerge: ligand exchange as well as ligand redox mechanisms are at play during clean-up and the precursor metal cation provides an energetic sink when it bonds to oxygen.

In the current investigation, building on the example of TMA, we look for an explanation of differences observed in the operation of different families of metal precursors: alkylamides, methyls and chlorides. We focus mainly on the clean-up of the arsenic (III) oxide component of the surface utilizing the $Hf[N(CH_3)_2]_4$ precursor during HfO_2 ALD. The choice of the surface model has been previously motivated and its structure and limitations have been described in detail [14]. The main emphasis here is on the interaction of the dimethylamido ligand (dma) with the oxide surface with a view to finding potential redox properties of this ligand. Based on the TMA findings, the metal cation is assumed to be redox inactive, and to combine with oxide anions to form a dielectric oxide. We postulate that formation of the dielectric oxide is the driving force for the clean-up effect and confront this by investigating the clean-up ability of precursors that are chemically different to TMA. Assuming these postulates allows us to define and separate the factors governing the clean-up effect. In this way, a set of general reactions is generated and a comparison can be made between a number of different precursors. In the end, this approach should help with assessing whether clean-up is a general effect, regardless of precursor being used.

2. Computational method & approach

Periodic density functional theory (DFT) at 0 K as implemented in the VASP package [15] was applied as a reliable method for computation of the ground state electronic structure and total energy of crystalline materials. We use the generalized gradient approximation (GGA) of Perdew and Wang (PW91) [16] for the exchange-correlation energy. The core electrons were described with ultrasoft pseudopotentials

(USPP) [17] projected into real space and valence electrons were described with a plane-wave basis with a kinetic energy cutoff of 396 eV. Geometry optimization was carried out with a sparse Monkhorst-Pack *k*-point sampling of reciprocal space. A conjugate-gradient algorithm was used for ionic relaxation with all ions relaxed until the forces on the ions were less than 0.02 eV/Å.

High accuracy was used for bulk oxide calculations: convergence of energies to 10^{-4} eV with respect to coordinates of ions and cells, 130% of the standard plane-wave cutoff energy, convergence with respect to *k*-point sampling. The total energy versus volume for all models of the bulk oxide structures was optimized resulting in equilibrium lattice parameters that agreed well with experiment (with deviation less than 2%) [18]. Lattice parameters and space groups, along with *k*-point sampling for these calculations are given in the supporting information. We used experimental lattice constants for the bulk model of *arsenolite* arsenic (III) oxide [19] since its crystalline structure did not allow us to perform cell shape optimization within DFT as explained in detail before [14]. Ions were fully relaxed within the fixed As_2O_3 cell and the structural parameters compared well with the experimental values. The *arsenolite*-As_2O_3 (010) surface is modeled by periodic slabs separated by 10 Å of vacuum. We use a 2×2 surface expansion that contains 1 layer totaling 8 molecular units of As_4O_6 (80 atoms) and a 2×2×1 *k*-point mesh for surface calculations. This surface is computed to have a surface energy below 0.02 J/m^2. Gaseous species (precursor molecules and gas phase products) were individually relaxed in a simulation box, cubic or rhombohedral, of dimensions 15×15×15 Å, with six *k*-points located at the edges of the first Brillouin zone. Geometrical parameters for all optimised gaseous molecules can be found in the supporting information.

For investigation of the ligand decomposition surface reactions we use the bare As_2O_3 (010) surface. For redox reactions differences in Bader atomic charges [20], Δq, are analyzed to determine the chemical state of intermediates and thus help in predicting a final product. The sign convention used in this paper is that $\Delta q < 0$ means loss (oxidation of an atom) and $\Delta q > 0$ means gain (reduction of an atom) of electron population on atoms taking part in the considered reaction. To study the stability of surface bound

intermediates we performed DFT molecular dynamics in the canonical ensemble at around 300° C for 0.4 ps. At the end of these simulations all surface intermediates were found to be bonded the same as their initial configuration, suggesting that no spontaneous reactions occur and that there are barriers to overcome on the potential energy surface for any following chemical transformations. We neglect the constant contribution to entropy (S) from solid surfaces with adsorbates since S^{trans} and S^{rot} for surfaces are approximately zero and S^{vib} is approximately constant during the reaction, $\Delta S^{vib} = 0$. Therefore $\Delta S = 0$ for surface reactions and the Gibbs free energy profiles closely resemble the DFT potential energy surfaces. Reaction energetics are computed with an estimated accuracy of 0.1 eV. Activation energies reported here were computed using the nudged elastic band method (NEB) [21]. We used up to 8 images for each reaction pathway. The damped molecular dynamics algorithm for ionic relaxation was found to be appropriate for the regarded system. Around 1000 steps were needed to converge forces on atoms to below 0.05 eV/Å.

In this investigation we consider the process where the adsorbed metal precursor molecules, with the general formula ML_n (M = Mg(II), Al(III), Ti(IV), Zr(IV), Hf(IV), Ta(V); L = $[N(Me)_2]^-$, $[Me]^-$, $[Cl]^-$; n – oxidation state of metal), undergo a series of clean-up transformations leading to removal of the native oxides of III-V substrates. As outlined in section 1, we propose that the main and most thermodynamically stable product of these transformations is a film of dielectric metal oxide with the general formula M_2O_n. (Thus, there is no reduction or oxidation of M). Another factor in the successful clean-up performance is affinity of the precursor ligand L to the III-V oxide substrate. We can describe formation of one O-M bond and subsequent transformations of the ligand on the sample III-V oxide surface (*i.e.* a clean-up process) with the following equation where || stands for surface bound species and g for gas-phase molecules:

(1) $||\text{As-O}|| + \frac{1}{n}\ ML_{n\,(g)} \rightarrow ||\text{O-}M_{\frac{1}{n}} + ||\text{As-}\textit{intermediates}$; with $\Delta E_{\text{clean-up}}$.

In the above equation we assume that the formed metal oxide is stoichiometric: upon increasing the coordination number of the metal centre to the native oxide oxygen, the coordination to the ligands

decreases and ligands are released to interact with the substrate. The equation also shows that *M*-O formation and interaction of ligands with As can be viewed as separate events, to a first approximation. Identification of these separate factors allows for an efficient description of interactions of the surface *intermediates* that are formed as a result of ligand decomposition, and of associated chemical processes that lead to formation of the clean-up products. Computing the *intermediates* from just one ligand should be computationally less expensive and easier to understand than computing the decomposition of the entire precursor molecule. Therefore, in this paper we take advantage of this methodology and reduce equation (1) to a description of chemical processes associated only with the interaction of one ligand with the substrate independent of *M*, as per the reaction:

(2) $||\text{As-O}|| + \text{H}L_{(g)} \rightarrow ||\text{O-H} + ||\text{As-}intermediates$; with ΔE_L.

A proton is included to ensure overall charge neutrality and so on the right hand side of the reaction a hydroxyl group ||O-H is formed. The formation of one *M*-O bond in equation (1) can then be described by the model reaction for various *M*:

(3) $\frac{1}{n}\ ML_{n\,(g)} + \frac{1}{2}\ \text{H}_2\text{O}_{\,(g)} \rightarrow \frac{1}{2n}\ M_2\text{O}_{n\,(\text{bulk})} + \text{H}L_{\,(g)}$; with ΔE_M,

which is the overall ALD reaction. Combination of the ligand reaction (2) and the metal-dependent correction (3) gives essentially reaction (1):

(4) $||\text{As-O}|| + \frac{1}{n}\ ML_{n\,(g)} \rightarrow M_{\frac{1}{n}}\text{O}_{\frac{1}{2}\,(\text{bulk})} + ||\text{As-}intermediates$; with $\Delta E'_{\text{clean-up}} = \Delta E_L + \Delta E_M$,

but at much lower computational effort. Therefore:

(5) $\Delta E_{\text{clean-up}} \approx \Delta E'_{\text{clean-up}}$.

Because of limitations of our current model, we cannot generally compute the complete energetics for each mechanism here. As we focus in this study on the decomposition of the dma ligand and its redox properties, our model naturally does not cover molecular or dissociative adsorption of the precursor and associated steric effects. Nevertheless, for validation purposes we performed explicit simulation of the dissociative adsorption of the whole precursor molecule according to equation (1). In Table 1 we compare energetics obtained for adsorption and ligand dissociation for three different precursors:

185 $Hf(NMe_2)_4$, $AlMe_3$, $TiCl_4$. The 'whole precursor' approach gives a $\Delta E_{clean\text{-}up}$ that agrees well with the
186 $\Delta E'_{clean\text{-}up}$ value from the 'ligand only' approach in all three cases, thereby strongly supporting the latter
187 approach. Additionally the 'whole precursor' approach for the $Hf(NMe_2)_4$ precursor was used for the
188 NEB calculation of activation energies, which is reported in the Results and Discussion section.
189
190 Table 1. Validation of the investigated model: energies $\Delta E_{clean\text{-}up}$ for reaction of precursor adsorption
191 and dissociation of the ligand from the metal center according to reaction ||As-O|| + $\frac{1}{n}$ $ML_{n\,(g)}$ → ||O-
192 $M_{\frac{1}{n}}$ + ||As-*L* compared to $\Delta E'_{clean\text{-}up}$ obtained from the model 'ligand only' reaction ||As-O|| + $\frac{1}{n}$ $ML_{n\,(g)}$
193 → $M_{\frac{1}{n}}O_{\frac{1}{2}\,(bulk)}$ + ||As-*L*. Surface models showing product of this reaction on the example of $Hf[N(Me_2]_4$
194 precursor are available in the supporting information. Simulations were performed using identical
195 computational parameters for both approaches.

Metal precursor	$\Delta E_{clean\text{-}up}$ [eV]	$\Delta E'_{clean\text{-}up}$ [eV]
$Hf(NMe_2)_4$	-1.0	-1.0
$AlMe_3$	-1.2	-1.3
$TiCl_4$	-0.2	-0.2

196
197 In section 3.1 thermodynamic energies are presented for formation of metal oxides from gas phase
198 precursors determined using DFT, ΔE_M (equation (3)). In the subsequent sections different types of
199 *intermediates* that are formed during clean-up as a result of decomposition of selected precursors are
200 examined and their structures are illustrated in Figure 2. Types of reactions included are: dissociation of
201 the precursor through scission of the *M-L* bond in section 3.2, decomposition of the dma ligand through
202 scission of the C-H and N-C bonds in section 3.3 and multiple decomposition steps combining these
203 elementary steps described in section 3.4. Energetics for the interaction of ligands with the substrate,
204 ΔE_L, is given in Table 2. The effectiveness of different metal precursors in performing clean-up of III-V
205 oxides is evaluated by correcting ΔE_L with ΔE_M (also Table 2). ΔE_M and ΔE_L along with overall $\Delta E'_{clean\text{-}}$

206 $_{up}$ are summarized in Figure 1 and Figure 3. A reaction scheme considered for the decomposition of the
207 dma ligand is illustrated in Figure 4. A series of proposed elementary steps can give rise to desorption of
208 multiple clean-up products. Based on the thermodynamic accessibility of these elementary surface steps
209 and some kinetic indications, we discuss in each section which clean-up mechanism and associated by-
210 product is competitive in the ALD process.

211 ## 3. Results and Discussion

212 ### *3.1. Formation of metal oxides from gas phase precursors*

213 Reaction (3) contains information about the reactivity of precursors towards formation of bulk oxide and
214 bonding changes upon elimination of ligands as H*L*. Computed energetics for a selection of metals and
215 ligands are summarized and illustrated in Figure 1. Values for reaction (3) can be found in Table 2
216 under $\Delta E'_{\text{clean-up}}$ for $\Delta E_L = 0$ eV (see equations (3) and (4)).

217

218 Figure 1. Computed energetics, ΔE_M, for formation of metal oxides from gas phase precursors ML_n (*x*
219 axis: *M* = Mg(II), Al(III), Ti(IV), Zr(IV), Hf(IV), Ta(V); *L* = $[N(Me)_2]^-$, $[Me]^-$, $[Cl]^-$; *n* = oxidation state
220 of metal) and water according to: $\frac{1}{n}\ ML_{n\,(g)} + \frac{1}{2}\ H_2O_{\,(g)} \rightarrow \frac{1}{2n}\ M_2O_{n\,(bulk)} + HL_{\,(g)}$ (equation (3)). Lines
221 are to guide the eye.

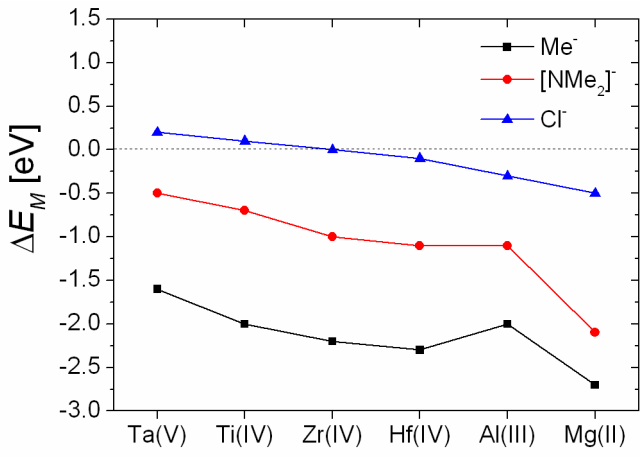

222

223

The energetics indicate that the most reactive precursor family for formation of metal oxides and elimination of H*L* are metal methyls. The most reactive of the six considered is $MgMe_2$ with ΔE_M = -2.7 eV per methyl ligand. The least reactive among the hypothetical methyl precursors is $TaMe_5$ with ΔE_M = -1.6 eV per Me for formation of Ta_2O_5. $AlMe_3$ with ΔE_M = -2.0 eV per Me presents similar reactivity to $TiMe_4$, not to $HfMe_4$ or $ZrMe_4$. Al, Hf and Zr alkylamides with $\Delta E_M \approx$ -1.0 eV per ligand have similar reactivity and the Ta and Ti alkylamides are slightly less reactive. The most reactive for formation of oxide among metal alkylamides is $Mg[N(CH_3)_2]_2$ with ΔE_M = -2.1 eV per alkylamide ligand. According to our computations the smallest driving force for formation of M_2O_n is shown by chloride precursors. ΔE_M for $L = Cl^-$ ranges from -0.5 eV per Cl for Mg to +0.2 eV per Cl for Ta. In general, the calculations reveal the following order of *M* reactivity, insensitive to the identity of *L*: Mg(II) > Hf(IV) ≈ Zr(IV) > Ti(IV) > Ta(V). The exception is Al(III) which is predicted to change its relative reactivity depending on the nature of *L*. Relative to the other metals, the Al cation is the most reactive when bonded to chloride ligands and the least reactive, with similar reactivity to Ti(IV), for $L = Me^-$. These trends are consistent with previous calculations [22].

Table 2. List of possible clean-up *intermediates*: **A-K**, **A'** and **A''** that are formed during ALD III-V substrate exposure to various metal precursors. Energies are in eV relative to ||As – O|| + H$L_{(g)}$ as per reaction (2) with L = $[N(Me)_2]^-$, Me^-, Cl^-. The effect of different M = Ta, Ti, Zr, Hf, Al, Mg is included by adding the correction ΔE_M obtained from reaction (3) (see section 2 for details).

L		products at surface:	ΔE_L	$\Delta E'_{\text{clean-up}}$ for M:					
				Ta	Ti	Zr	Hf	Al	Mg
$[N(Me)_2]^-$		$\|\|As – O\|\| + HNMe_{2\,(g)}$	0.0	-0.5	-0.7	-1.0	-1.1	-1.1	-2.1
	A	$\|\|O – H + \|\|As – NMe_2$	+0.1	-0.4	-0.6	-0.9	-1.0	-1.0	-2.0
	B	$2\|\|O – H + \|\|As – N(Me)CH_2 – As\|\|$	+0.6	+0.1	-0.1	-0.4	-0.5	-0.5	-1.5
	C	$2\|\|O – H + \|\|As – N(Me)CH_2 – O\|\| + 2e^-$	+1.3	+0.8	+0.6	+0.3	+0.2	+0.2	-0.8
	D	$\|\|O – H + \|\|As – N(Me)CH_2 – As\|\| + \|\|As – H - 2e^-$	+2.1	+1.6	+1.4	+1.1	+1.0	+1.0	0.0
	E	$\|\|O – H + \|\|As – N(Me)CH_2 – O\|\| + \|\|As – H$	+1.2	+0.7	+0.5	+0.2	0.1	0.1	-0.9
	F	$\|\|O – H + \|\|As = NMe + \|\|O – Me$	+1.5	+1.0	+0.8	+0.5	+0.4	+0.4	-0.6
	G	$\|\|O – H + \|\|As = NMe + \|\|As – Me - 2e^-$	+1.6	+1.1	+0.9	+0.6	+0.5	+0.5	-0.5
	H	$3\|\|O – H + \|\|As – N(CH_2 – As\|\|)_2$	+1.3	+0.8	+0.6	+0.3	+0.2	+0.2	-0.8
	I	$4\|\|O – H + \|\|As = NCH=CH_2 + 2e^-$	+2.2	+1.7	+1.5	+1.2	+1.1	+1.1	+0.1
	J	$2\|\|O – H + \|\|As – N=CH_2 + \|\|As – Me$	+0.9	+0.4	+0.2	-0.1	-0.2	-0.2	-1.2
	K	$3\|\|O – H + \|\|As – N=CH – As\|\| + \|\|As – Me$	+1.9	+1.4	+1.2	+0.9	+0.8	+0.8	-0.2
$[Me]^-$		$\|\|As – O\|\| + CH_{4\,(g)}$	0.0	-1.6	-2.0	-2.2	-2.3	-2.0	-2.7
	A'	$\|\|O – H + \|\|As – Me$	+0.7	-0.9	-1.3	-1.5	-1.6	-1.3	-2.0
$[Cl]^-$		$\|\|As – O\|\| + HCl_{(g)}$	0.0	+0.2	+0.1	0.0	-0.1	-0.3	-0.5
	A''	$\|\|O – H + \|\|As – Cl$	-0.3	-0.1	-0.2	-0.3	-0.4	-0.6	-0.9

3.2. Dissociation of ligand by M-L scission

By calculating DFT energies for dissociation of the ligand from the metal center, we investigate the affinity of the ligand to the oxide to be cleaned-up. This gives us $\Delta E'_{\text{clean-up}}$ for the elementary step that leads to a ligand exchange mechanism. The elementary steps that we have considered involve the transfer of a dimethylamide, methyl and chloride group to the surface As atom in structures **A**, **A'** and

A'' respectively, shown in Figure 2. Energetics for formation of intermediate **A** show that the alkylamide ligand can readily dissociate from the *M* center to the available As site and form a thermodynamically stable product ||As – $N(CH_3)_2$ plus oxide of *M* (see Table 2 and Figure 3 for energetics). According to reaction (2) and correction for the *M*-O bond formation, reaction (3), this ligand transfer process is exothermic for all considered metals. The energy for this reaction ranges from -0.4 eV per ligand for $Ta[N(CH_3)_2]_5$ to -2.0 eV for $Mg[N(CH_3)_2]_2$. This reaction is very facile with a computed activation energy of just +0.1 eV, and so it will proceed until the surface is saturated with ||As – $N(CH_3)_2$ species (the reaction profile for the corresponding reaction of the whole precursor is available in the supporting information).

Figure 2. Surface models for As_2O_3 and decomposition species of metal methyls, **A'**, metal chlorides, **A''**, and metal alkylamides, **A**-**K**. Stick representation: purple As, red O, white H, gray C, green Cl, blue N. Selected bond lengths are given in Å. Thin lines show adjacent substrate atoms.

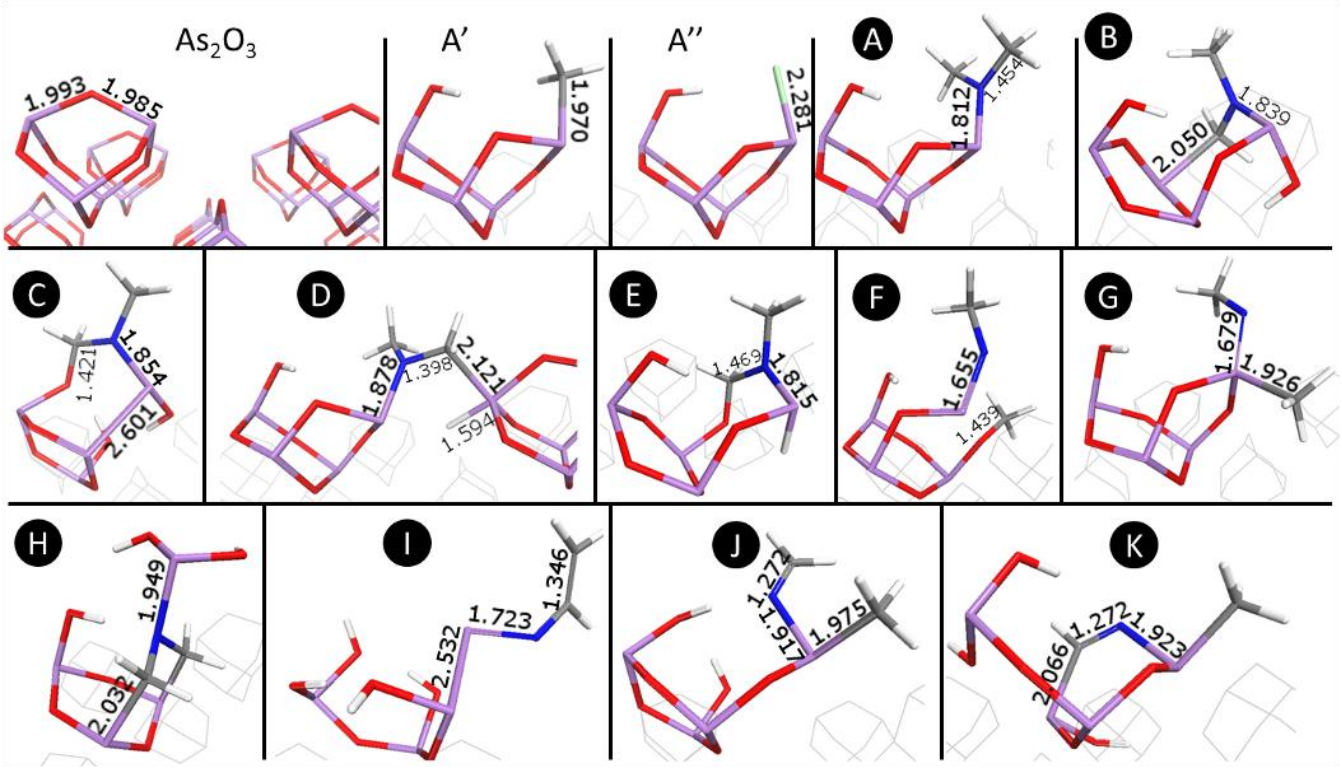

Figure 3. Computed energetics for surface intermediates, **A**-**K**, which are formed during clean-up of As_2O_3. As listed in Table 2, **A**, **A'** and **A''** are surface products of precursor decomposition through scission of *M*-*L* bond (*M* = Mg(II), Al(III), Ti(IV), Zr(IV), Hf(IV), Ta(V)) for *L* = $[N(Me)_2]^-$, $[Me]^-$, $[Cl]^-$ respectively; **B**-**E** are surface products of decomposition of $[N(Me)_2]^-$ through scission of C-H bond; **F** and **G** surface products of decomposition of $[N(Me)_2]^-$ through scission of N-C bond; **H**-**K** are surface products when further decomposition occurs through scission of both C-H and N-C bonds. ΔE_L (equation (2)) describes interaction of the ligand *L* with the As_2O_3 substrate (black datapoints). It is subsequently corrected with ΔE_M (equation (3)) and gives overall $\Delta E'_{clean\text{-}up}$ for various *M* (equation (4)). Lines are to guide the eye and do not imply a reaction sequence (see instead Figure 4).

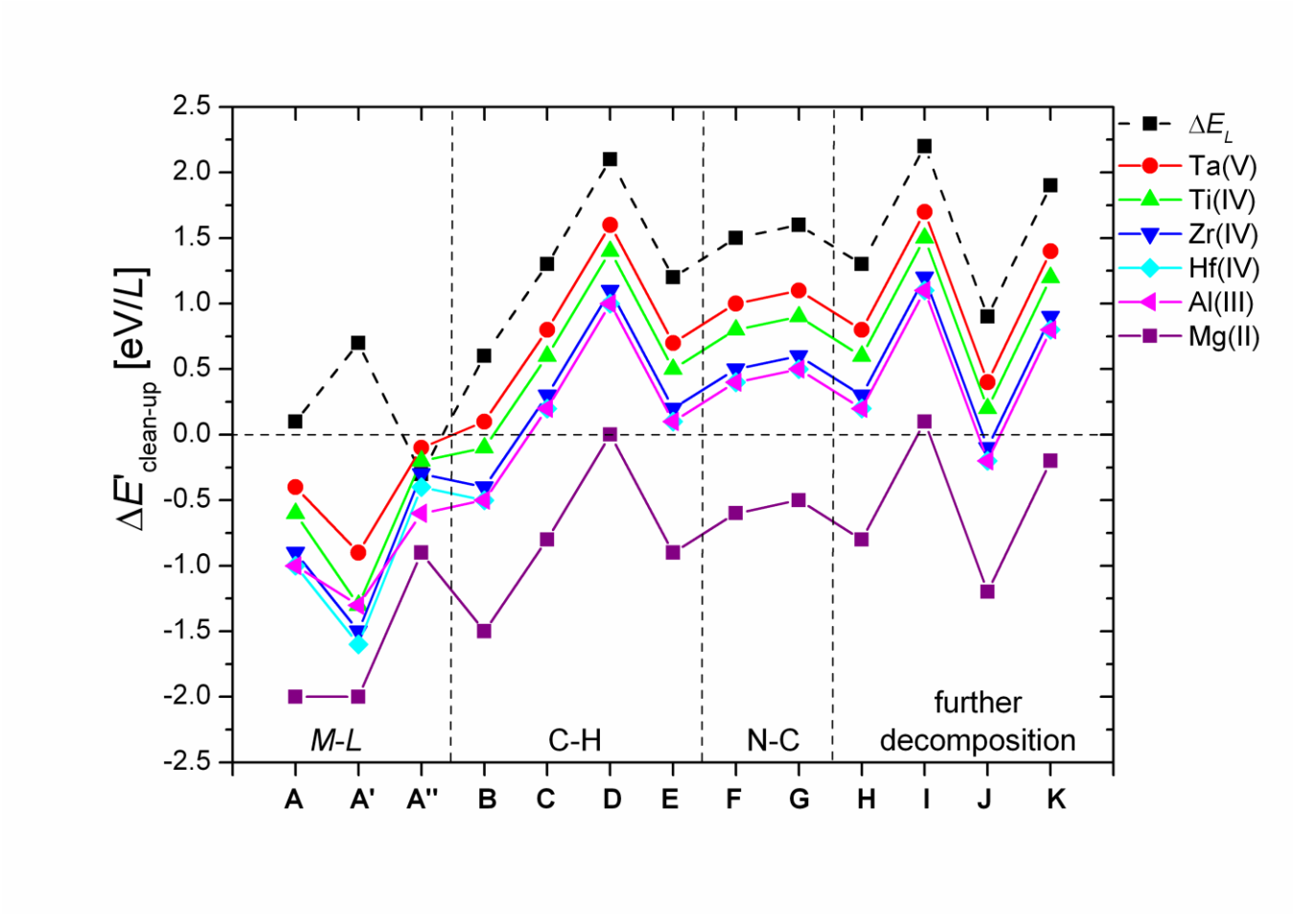

Energetics show that the methyl ligand is very reactive towards the arsenic oxide substrate and more reactive than alkylamide (**A'** Figure 3). The energy ranges from -0.9 eV for $Ta(CH_3)_5$ to -2.0 eV for $Mg(CH_3)_2$. The energy for exchange of a Cl^- ligand between the precursor metal center and the native

oxide, with product **A''** in Figure 2, ranges from -0.1 eV for $TaCl_5$ to -0.9 eV for $MgCl_2$, indicating that it is less thermodynamically favored than for alkylamides and methyls.

Sufficient concentration of these As – *L* groups may lead to formation of AsL_3: tris(dimethylamino)arsine, TDMAAs, $As[N(CH_3)_2]_3$; trimethylarsine, $As(CH_3)_3$ and arsenic trichloride $AsCl_3$, as volatile products in processes utilizing alkylamides, methyl and chloride precursors respectively. Desorption of these molecules means that As_2O_3 has been transformed into M_2O_n, *i.e.* clean-up. Indeed, this ligand transfer mechanism has been proposed by others [3a, 8] to explain the clean-up effect. Experimental study clearly shows enhancement of the clean-up process with increasing temperature when metal alkylamides are used [5, 23]. Even though the first step of the ligand exchange reaction is extremely facile, both thermodynamically and kinetically, significant kinetic requirements may originate from steric effects in subsequent steps. There was evidence for this in our previous study for TMA, where we showed that the rate limiting step for the ligand transfer process could be crowding of methyl ligands at one surface site [24]. We suspect that this process can be even more difficult for the bulkier alkylamides. Thus, steric effects may have a pronounced influence on the kinetics of ligand transfer to TDMAAs, which may stop this reaction before going to completion, and promote ligand decomposition instead. In fact, TDMAAs is known to thermally decompose on the GaAs surface [25]. Therefore, it is reasonable to suspect that the alkylamide can decompose, or partially decompose, in contact with the native oxide surface, and give rise to other clean-up products rather than form TDMAAs. Ligand decomposition is investigated in subsequent sections.

In the case of chlorides, although they are successfully used in ALD of different metal oxides, there is no agreement in the literature about their interfacial self-cleaning abilities [3b, 4a, 10]. One reason may be the lower driving force towards formation of the metal oxide dielectric; Figure 1 shows that formation of the metal oxide during clean-up is an important factor in case of alkylamides and methyls, but a minor factor in the case of chlorides (ΔE_M ranges +0.2 to -0.5 eV). Therefore, we suggest that chloride chemistry is different. Most of the metal chlorides are weak Lewis acids. Their electrophilic

312 characteristic allows them to form Lewis adducts like $TaOCl_3$, complexes like $[TiCl_6]^{2-}$ or even
313 hydrates, *e.g.* $MgCl_2(H_2O)_x$ [26]. Formation of oxychlorides, e.g. $TiOCl_2$, or even hydroxychlorides,
314 $TiCl_3OH$, during clean-up with $TiCl_4$ for TiO_2 deposition, could explain observed removal of O and
315 surface passivation with Cl [4a]. As proposed before, clean-up with this ligand can be accounted for via an
316 agglomeration reaction mechanism [3b].
317 Ligand affinity for Ga and In is discussed in section 3.5 .

318 ### *3.3. Decomposition of dma ligand*

319 For the following consideration of decomposition processes of alkylamide ligand on the example of
320 dimethylamide we use the highly stable product **A** ||As – $N(CH_3)_2$, as a starting species for further clean-
321 up transformations **B**-**K**. Decomposition of the alkylamide ligand is possible via activation of a C-H
322 bond, releasing anionic or cationic H, or of an N-C bond, releasing anionic or cationic CH_3 as
323 schematically shown in Figure 4. In this section we examine mechanistic paths for these H and CH_3
324 moieties to attack As and O sites. We consider all possible reactions and highlight redox processes that
325 may enhance the clean-up effect.

326
327
328
329
330
331
332
333
334
335
336
337

Figure 4. Reaction scheme for decomposition of dimethylamido ligand $[–N(CH_3)_2]^-$ on metal oxide surfaces (species **A**-**K**). Notation: '$–H^{+/-}$' means dissociation of proton/hydride from ligand to the surface; '$–Me^{+/-}$' means dissociation of methylium/methanide group from ligand to the surface; '$+2e^-$' means oxidation of ligand by surface (reduction of surface by ligand); '$-2e^-$' means reduction of ligand by surface (oxidation of surface by ligand).

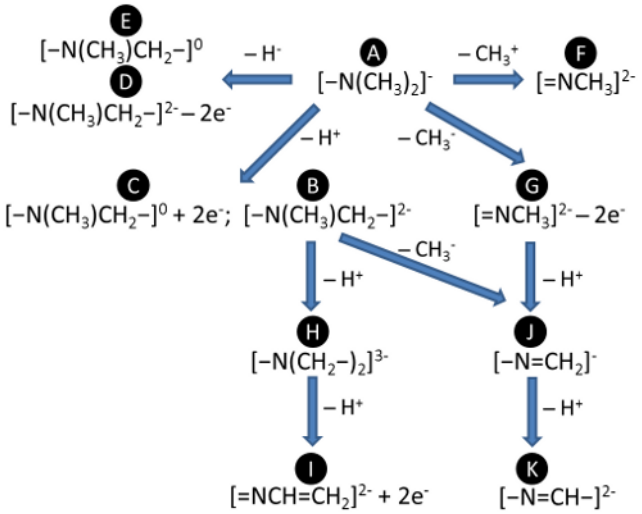

3.3.1. C-H scission and H elimination (B-E)

The C-H bond of the ligand is weakened by the electron density of the lone pair of electrons on the neighboring N atom, so that H α to the N atom can dissociate and bond to an available surface site. First we investigate scission of the C-H bond and formation of an O-H bond in the intermediate **B** shown in Figure 2. Our calculations show that upon the proton (H^+) transfer from a ligand to a surface O atom, the As-O bond is broken. The electronic density around the C atom in the remaining methylene (CH_2) moiety of the ligand increases by $\Delta q = +1.5e$. This Lewis basic C atom can interact with the surface As cation that lost coordination to the O atom. The bond formed between the As atom and the C atom is 2.0 Å long which is typical of single As-C bond. As a result a N-methylmethylenimido ion ($[–N(Me)CH_2–]^{2-}$) is attached to the surface. Our attempts to find a competitive minimum for the N-methylmethylenimido ligand with tricoordinated N atom featuring a N=C double bond (*i.e.* $[–N(Me)=CH_2]^-$) were not successful. The thermodynamically stable state preserves tricoordinated N and tetrahedral C. This process is the most exothermic of the decomposition processes with a calculated

$\Delta E'_{clean\text{-}up}$ ranging from +0.1 eV for $Ta[N(CH_3)_2]_5$ to -1.5 eV for $Mg[N(CH_3)_2]_2$ (Table 2, **B**). An activation energy of around +1.4 eV is computed for the example of $Hf[N(CH_3)_2]_4$ where $\Delta E'_{clean\text{-}up}$=-0.5 eV (the reaction profile for the corresponding reaction of the whole precursor is available in the supporting information).

We also examine the redox process mediated by ligand attack of the CH_2 moiety onto the O site, instead of the As site, to form product **C** (Figure 2). This is analogous to the migration of CH_3 from As to O that we observed to be responsible for clean-up with TMA [14]. In this elementary step two As-O bonds are broken, promoting formation of the O-H (1.0 Å) bond and the O-C bond (1.4 Å). Two electron-deficient surface metal cations are forced to interact and as a result a metallic As-As dimer is formed along with the intermediate ||As – NCH_3CH_2 – O||. Electrons are transferred to surface arsenic (+1.0*e* and +1.1*e* on the dimer atoms) from the C atom of CH_2 (-1.6*e*) but also from N (-0.5*e*), elongating the N-As bond by around 2% as compared to structure **A**. Decomposition of the alkylamide via this process is thus reducing the As oxide surface and contributing to clean-up. This oxidation of the C atom is endothermic for most of the precursors: tantalum, titanium, zirconium amides (+0.8, +0.6, +0.3 eV respectively), almost neutral for hafnium amide (+0.1 eV) and exothermic for magnesium amide (-0.8 eV) according to equations (2) + (3) ($\Delta E'_{clean\text{-}up}$, Table 2). It is less favorable than formation of the As-C bond in the structure **B** described above.

For completeness we studied scission of the C-H bond and the transfer of H to an As site. This process essentially involves hydride (H^-) dissociation from the alkylamide ligand and formation of products **D** and **E** with structures illustrated in Figure 2. In the intermediate **D** two new bonds are created: As-H and As-C, increasing the coordination number of the As atom from three to five. Formation of these two bonds is expected to cause the withdrawal of the electronic density from the oxide substrate and so its local oxidation (see scheme in Figure 4). Charge analysis suggests a decrease in electronic populations by only -1.0*e* on the oxidised pentacoordinated As and an increase of +1.0*e* on the H atom bonded to this arsenic. The absence of charge transfer between this arsenic and CH_2 suggests some charge retraction that is explained as follows. The CH_2 moiety of the created surface product ||As – $N(Me)CH_2$

– As|| becomes more Lewis acidic (-0.4*e* on the C atom) and the N atom more Lewis basic (+0.5*e*), attracting each other (4% shorter N-CH_2 bond, relative to the same bond in **B**) and repelling bonded arsenic atoms (both: As-N and As-CH_2 bonds are elongated by 4%, relative to the same bonds in **B** or **C**). This indicates that desorption of the N-methylmethylenimido ligand as neutral Me–N=CH_2 should be preferred over formation of the dianion ($[–N(Me)CH_2–]^{2-}$ and substrate oxidation. The oxidation of As upon hydride dissociation is not favorable. In fact this is one of the least favorable processes that we have computed with energy ranging from +1.6 eV to +1.0 eV for almost all of the precursors and energetically neutral only for $Mg[N(CH_3)_2]_2$. We observe that no As-O bond is broken in this elementary process, *i.e.* it does not contribute to clean-up.

Our results indicate that energy for hydride dissociation can be lowered by 0.9 eV when this process is accompanied by oxidation of the C atom and formation of the surface product **E**: ||As – NCH_3CH_2 – O|| + ||As – H. In this case As-H and O-C bonds are formed breaking one As-O bond (see Figure 2). We note that electronic densities are withdrawn from the O-CH_2-N entity (-1.0*e*) by the newly-formed hydride (+1.0*e*) and there is no charge transfer to the substrate. The attack of CH_2 onto the O site and transfer of H^- to the As site is slightly endothermic for most of the precursors (+0.7 to +0.1 eV) and exothermic for the magnesium precursor (-0.9 eV).

DFT calculations show that decomposition of alkylamide ligand through scission of the C-H bond α to N is thermodynamically feasible, but requires quite high activation energy. This pathway is often referred to in the literature as β- H elimination [27]. Most likely this process will result in hydroxylation of the native oxides and formation of C-As(Ga, In) bonds (**B**). A possible volatile product of this clean-up transformation is N-methyl methyleneimine (MMI). Desorption of imine in the considered system requires reorganization in the electronic density with the formation of an N=C double bond and cleavage of As-N and As-C bonds, which is consistent with a high activation energy (+1.4 eV for the Hf case; see above). Simultaneously, charge transfer to the surface As should occur resulting in formation of metallic As-As bonds. We calculate that desorption of imine according to the reaction: ||As –

NCH_3CH_2 – As|| → ||As-As|| + CH_3NCH_2 $_{(g)}$ costs +0.7 eV relative to formation of **B**. Thus, the computed reaction energies and high activation energy for the first step suggest that this clean-up pathway producing imine needs elevated temperature for activation.

The weakening effect of the N-lone pair on the C-H bonds in the α position has been observed in vibrational spectroscopy, where an unusually low frequency of vibration of the C-H mode in TDMAH has been reported [28]. The C-H dissociation is possible already upon adsorption of alkylamide precursors onto silicon substrates at very low temperature of 220 K [29]. As mentioned in the previous section MMI is a detected product of etching GaAs surface by TDMAAs [25a]. Several reports can be found where metal alkylamides are shown to decompose to produce imine and amine [30]. We show here that H elimination can occur from a ligand that has migrated to the native oxide surface (**A** → **B**). Product **B** can then undergo other transformations **B** → **H**-**K**, leading to different clean-up products as described later, or desorption of imine can occur. Either process leads to arsenic oxide removal and/or reduction to metallic arsenic, and so may contribute to the clean-up effect.

Another clean-up product that can arise from H elimination in the structures **D** and **E** is arsine, AsH_3. However, the unfavourable energetics computed by DFT for elementary steps leading to surface functionalization with ||As – H groups suggests that formation of arsine from intermediate **D** or **E** is a minor clean-up channel.

3.3.2. N-C scission (F-G)

We next examined possible pathways for CH_3 dissociation resulting with products **F** and **G** (for pathways see Figure 4, for structures of products Figure 2). First we considered activation of the N-C bond in the presence of the available Lewis basic O site of the substrate (**F**). As the CH_3 group coordinated to the N atom in the alkylamide ligand has Lewis acidic character (formally CH_3^+, methylium cation), we expect no redox during transfer to the substrate in this step. Upon this transfer the As-O bond is broken, promoting formation of a double bond between the As and N atoms (1.7 Å). Our results indicate that the reaction along this pathway is moderately endothermic with a

thermodynamic energy of +1.0 to +0.4 eV for Ta, Ti, Zr, Hf, Al precursors and exothermic by -0.6 eV for the Mg precursor ($\Delta E'_{\text{clean-up}}$. Table 2).

Another possibility is for the CH_3 moiety to attack an As surface site (**G**). The DFT calculations show that, similarly, an As=N double bond is formed, but As-O bonds are not affected. We observe oxidation of the As atom (-1.9*e*), which is now pentacoordinated, and reduction of the C atom of the dissociated CH_3 moiety (+1.9*e*), consistent with transfer as CH_3^- (methanide anion). This elementary step is therefore the reverse of clean-up. The bond formed between the C atom and the As atom is 1.9 Å long. This decomposition structure is a little more unstable than **F** with respect to reactants, at a calculated energy difference of +0.1 eV relative to the energy for formation of product **F**.

Pathways involving dissociation of the methyl group lead to functionalization of the surface with ||O – CH_3 (**F**) or formation of the ||As – CH_3 groups (**G**) along with the ||As = NCH_3 fragment. This can thus lead to desorption of gaseous dimethyl ether, $O(CH_3)_2$, or trismethylarsine, $As(CH_3)_3$. Additionally, if a source of protons is present, methane CH_4 can be formed from ||As – CH_3. However, our calculations show that elementary steps for **F** and **G** formation that could give dimethyl ether or trismethylarsine as clean-up products are less competitive when compared to the elementary steps leading to formation of TDMAAs or MMI (**A** or **B**, see Table 2). During ALD of metal oxide films, protons can derive from the H_2O pulse, but are supposedly eliminated in reaction with alkylamide ligands to produce amine, the main ALD product. ||O-H groups are also formed during the H elimination process investigated above. We will see later that the sequence of production of **B** and **G** *intermediates* is competitive and can directly lead to methane production.

3.4. Further decomposition of dma ligand

3.4.1. Multiple redox steps – dehydrogenation H-I

Based on the results shown above, we assume that the main reaction channel for the elimination of H atoms from alkylamide ligands on the oxide substrate is formation of the surface hydroxide and carbon-arsenic bound *intermediate* as in product **B**. In this section we investigate the most stable products of successive dehydrogenation of the alkylamide ligand.

459 The stability of the surface intermediate **H** decreases by about 0.7 eV relative to **B** after a second proton
460 transfer. The electronic density increases on both C atoms (+1.2*e* and +1.3*e*) and a total of two protons
461 are transferred to the oxide surface. There are now two CH_2 entities that form bonds with acidic As
462 atoms through basic C atoms. A loss of electronic density on N of -0.5*e* is observed in Bader analysis.
463 This affects the As-N bond, which is weakened (about 8% longer than the As-N bond in product **B**)
464 suggesting that the π character of this bond decreases. The lone pair of electrons on N is no longer
465 stabilized and N becomes nearly pyramidal in this structure (see Figure 2). This process requires energy
466 and so it is clear that it requires some thermal activation.
467 Further dehydrogenation is possible via carbon disproportionation yielding a methylidyne fragment
468 (HC) that inserts into the C-N bond in the intermediate **I**. The surface product features a double bond
469 between As and N (1.7 Å) that is now bound to a vinyl moiety $CH=CH_2$ (C=C bond length: 1.3 Å).
470 Three hydroxide groups and an As-As dimer with the bond length of 2.5 Å are formed at the expense of
471 four As-O bonds. Bader analysis confirms reduction of the dimer As atoms (+1.1*e* and +1.4*e* for the As
472 atoms bound to N) which means that this reaction contributes to clean-up. We also observe
473 disproportionation of charge between C atoms (increase of electronic population on methylene group of
474 +0.6*e* and decrease on methylidyne group of -0.3*e* relative to populations on methyl groups in amide
475 ligand in structure **A**). We note some charge transfer to the N atom of +0.5*e*. Formation of an
476 $[=NCH=CH_2]^{2-}$ adsorbate is the most endothermic of the considered processes (+1.6 eV relative to **B**
477 formation).
478 Our computations thus show that successive dehydrogenation becomes progressively less favored. It
479 may result in the formation of the following volatile products: imine from species **B** as mentioned
480 above; aziridine, $HN(CH_2)_2$, from **H**; ethylene, C_2H_4, and subsequently molecular nitrogen, N_2, from **I**.
481 The energetics for pathways leading to desorption of these species suggest that this is only possible
482 through thermal activation – moderate temperatures for imine formation and high temperatures for
483 desorption of molecular nitrogen.

Aziridine may be produced from structure **H** by a reaction of cleaving As-C bonds, forming a C-C bond (for this process we calculate +0.5 eV relative to formation of **H**), subsequent coupling with adjacent protons if available and desorption, all of which has a DFT energy of just +0.3 eV relative to **H**. This contributes to clean-up, leaving the surface with metallic As-As bonds according to: $||As - N(CH_2 - As||)_2 + ||O - H \rightarrow ||As - O|| + ||As - As|| + HN(CH_2)_{2\ (g)}$. The rate limiting step may be breaking As-C and forming a three membered C-C-N ring. Aziridine is one of the stable products detected in the *in situ* mass spectroscopy experiment of thermal decomposition of TDMAAs below 450°C [30b].

C_2H_4 was detected as a desorption product originating from secondary surface reactions when a tantalum surface was exposed to $Ta[N(CH_3)_2]_5$ at 550 K [27]. One of the proposed mechanisms envisages dehydrogenation of methyleneimido intermediates, insertion of a methylidyne moiety into the carbon-nitrogen bond and subsequent hydrogenation of the vinyl fragment to produce ethylene and leave an adsorbed N atom [27]. We suggest that, on the reducible arsenic oxide substrate following coupling of adsorbed N atoms to form N_2 could be possible at highly elevated temperatures, which would result in clean-up according to: $2\ ||As = NCH=CH_2 + 2\ ||O - H \rightarrow ||As - As|| + 2\ C_2H_{4\ (g)} + N_{2\ (g)}$.

3.4.2. Multiple redox steps J-K

In this section we study sequences of CH_3 dissociation and alkylamide dehydrogenation reactions that give rise to new clean-up products. Assuming, as previously, that the most probable pathway for alkylamide dehydrogenation is arsenic oxide hydroxylation, we can consider pathways where the CH_3 group formally dissociates either as the methylium cation or as the methanide anion (as the above investigation of processes producing **F** and **G** revealed a competition between them). Here we show the most stable products of these reactions. All other possible reactions can be found in the supporting information.

Our investigations suggest that the more stable products are those formed during reactions that do not involve charge transfer to the oxide substrate. For instance, dehydrogenation of the alkylamide ligand followed by dissociation of the methanide anion in structure **J** (Figure 1) is preferred over dissociation of the methylium cation that combined with proton dissociation results in substrate reduction: [–

510 $N(CH_3)_2]^- \rightarrow [–N=CH_2]^- + [CH_3]^+ + [H]^+ + 2e^-$ (not showed in Figure 1). The step leading to product **J** is
511 among the few steps that we find to be exothermic or neutral at 0 K for most of the regarded precursors
512 (Table 2). The reorganized electron density in the proton dissociation process (see section 3.3.1 for
513 description of the proton elimination process in structure **B**) can be attracted by a CH_3 group instead of a
514 CH_2 group. Bader analysis shows an increase in the electronic populations on the C atom of CH_3
515 (+1.9*e*) and decrease on the C atom belonging to the methylene moiety (-1.2*e*). The acidic methylene
516 forms a double bond with the N atom (1.3 Å), instead of bonding to surface cation like in structure **B**.
517 The basic methanide bonds with the As atom (2.0 Å). We note some increase of electronic density on
518 the N atom that is now even more basic (+0.5*e*) than in the original alkylamide ligand in structure **A**.
519 Proton dissociation accompanied by the formation of the methanide anion could be a low temperature
520 channel for the formation of CH_4. According to our computations formation of methane from surface
521 intermediate **J** is slightly exothermic with energy -0.1 eV (neglecting entropy). CH_4 was observed in
522 some studies as a product of decomposition of the amido ligands. Infrared (IR) spectroscopy and
523 temperature-programmed desorption (TPD) investigations of $Ti[N(CH_3)_2]_4$ on a Si substrate showed that
524 methane desorbs at temperatures below 400 K [29b]. In the same study DFT calculations suggest that
525 facile generation of methane right above room temperature is due to the surface activation of C – H and
526 C – N bonds of amido ligand. In the thermal chemistry investigation of $Ta[N(CH_3)_2]_5$ CH_4 is a
527 decomposition product detected throughout the studied temperature range up to 600 K [27]. Our DFT
528 results suggest that scission of the N-C bond is triggered by the H elimination process on the oxide
529 substrate and thermodynamically is not as demanding as other decomposition processes. Although
530 formation of methane is plausible, desorption of this chemical alone from the oxidised III-V system
531 does not directly result in self-cleaning. In this pathway methane is formed according to: ||As – Me + ||O
532 – H → ||As – O|| + CH_4, so arsenic oxygen bonds are formed. However, other products can arise as a
533 consequence of saturation of the native oxide surface with $[–N=CH_2]^-$ groups after CH_4 desorption in
534 species **J**: C_2H_4 and subsequently N_2. Eventual desorption of CH_4, C_2H_4 and N_2 would finally lead to
535 clean-up resulting in reduction of arsenic oxide to metallic arsenic, but involving multiple redox steps: 2

536 ||As – N=CH_2 → ||As – As|| + C_2H_4 $_{(g)}$ + N_2 $_{(g)}$. This process requires energy to break the double bond
537 between N and C atoms, combining two CH_2 groups and two N moieties on the surface. As remarked in
538 our discussion of possible products arising from *intermediate* **I**, processes involving multiple redox
539 steps are presumably possible at highly elevated temperatures.
540 Further dehydrogenation of the methylene group in the $[–N=CH_2]^-$ adsorbate described above, yields a
541 methylidyne (CH^+) ion in surface product **K**. This is less favored by +1.0 eV relative to previous
542 process **J** (see Table 2). Proton dissociation to another O site renews C basicity (+1.0*e* with respect to
543 the $[–N=CH_2]^-$ adsorbate) that now can attack another As site. The $[–N=CH–]^{2-}$ ion is bound to surface
544 arsenic atoms through N and C, forming bonds 1.9 Å and 2.0 Å long respectively (**K** Figure 1).
545 Generation of the $[–N=CH–]^{2-}$ surface intermediate can directly lead to desorption of hydrogen cyanide,
546 HCN, another clean-up product: ||As – N=CH – As|| → ||As – As|| + HCN $_{(g)}$. HCN was detected to
547 desorb at 600 K during tantalum alkylamide exposure to a tantalum substrate [27].

548 ### *3.5 Effect of substrate on clean-up*

549 Our model supposes that clean-up can be achieved by successive dissociation of ligands from the
550 absorbed precursor. One can expect that the $M – L$ bond can be easily activated on the oxide surface
551 when the substrate metal oxide is less stable than the deposited metal oxide M_2O_n. The metal center of
552 the precursor then becomes chemically active towards penetrating the III-V oxide substrate and
553 scavenging the oxygen. A similar technique is used for equivalent-oxide-thickness scaling for
554 complementary metal–oxide–semiconductor devices [31]. With different variations scaling is achieved via
555 a scavenging reaction between the scavenging element (metal) and SiO_2 and the driving force is also
556 formation of the metal oxide rather than maintaining SiO_2. We showed previously that the driving force
557 of the clean-up effect is removing As(Ga, In) – O bonds and forming M – O bonds [14, 31]. As has lower
558 electropositivity and therefore lower affinity to O than the metals considered: Mg, Hf, Zr, Ti, Ta and Al.
559 In thermodynamic equilibrium, formation of any of the oxides of these metals is assumed to be favored
560 over formation of the As oxide. DFT energetics for the ligand exchange mechanism supports this
561 supposition, independent of the ligand in use (see Figure 3 **A**, **A'** and **A''**). Among the III-V elements

(As, Ga, In) it is again As that has the lowest electropositivity and forms the weakest oxides. To emphasize this we calculate from first principles bulk energies for ligand exchange between the regarded precursors and Ga(III) and In(III) native oxides and compare them with the exchange energy for As(III/V) native oxide:

(6) $\frac{1}{n} ML_{n\ (g)} + \frac{1}{2m} N_2O_{m\ (\text{bulk})} \rightarrow \frac{1}{2n} M_2O_{n\ (\text{bulk})} + \frac{1}{m} NL_{3\ (g)}$, with ΔE_{L_ex}, where N = As(III), As(V), Ga(III), In(III); m = oxidation state of N.

Figure 5 shows the energetics for the above reaction on the example of alkylamide precursors (L = $[NMe_2]^-$). It is clearly seen that As_2O_3 is the weakest and the most reactive among these native oxides towards exchanging O with ligands and therefore is the easiest to clean-up. It seems that In oxide resists clean-up more than Ga oxide and is less likely to bind to ligands at the surface. As(III) and As(V) oxides are seen to have similar reactivity for ligand exchange, with the exception of $Al[NMe_2]_3$ that seems to have greater affinity for As(III). We observe no oxidation state dependency for the ligand exchange mechanism, contrary to the suggestion of Hinkle *et al* [8]. This result holds true for different ligands (see supporting information).

584 Figure 5. Computed energetics for ligand exchange of alkylamide between precursor metal center and
585 bulk III-V oxide: As_2O_3, As_2O_5, Ga_2O_3 and In_2O_3 according to: $\frac{1}{n} ML_{n\ (g)} + \frac{1}{2m} N_2O_{m\ (bulk)} \rightarrow \frac{1}{2n} M_2O_{n\ (bulk)} + \frac{1}{m} NL_{3\ (g)}$ for M = Mg(II), Al(III), Ti(IV), Zr(IV), Hf(IV), Ta(V), L = $[N(Me)_2]^-$; n = oxidation
586 state of M; N = As(III), As(V), Ga(III), In(III); m = oxidation state of N. Lines are to guide the eye.

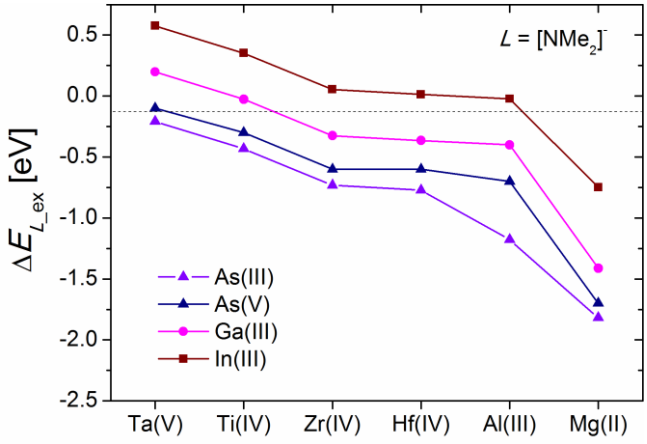

588

589

590 Additionally, ligands left on the surface can enhance the clean-up effect by interacting with the substrate
591 and this depends on the affinity of the ligand to the substrate and on the chemical character of the
592 substrate. We consider first ligand affinity. Metalloid oxides, like AsO_x, are susceptible to reduction in
593 contact with reducing agents, *e.g.* by the methanide anion Me^- in TMA as we showed previously [14] or by
594 CH_2 from deprotonated alkylamide (section 3.3.1, **C**). Self-cleaning by TMA was shown to be governed
595 by mobility of the methyl group, which undergoes oxidation, transferring electrons to the surface.
596 Various elementary steps were found to be thermodynamically competitive and to lead to a surprising
597 range of by-products. However, dma $[NMe_2]^-$ and chloride Cl^- anions are not as strong reducing agents
598 as Me^-. This is supported by DFT energies, shown in Figure 6, for reactions of transferring those ligands
599 from the metal center of the precursor to a surface O site on the As_2O_3 substrate. Formation of ||O – L
600 surface intermediates causes reduction of metalloid oxides:

601 **(7)** 2 ||As-O|| + $\frac{1}{n} ML_{n\ (g)} \rightarrow M_{\frac{1}{n}}O_{\frac{1}{2}\ (bulk)}$ + ||O-L + ||As-As|| with ΔE_{L_ox}.

In Figure 6 we can see that the chloride ligand, almost independently of which metal center it is bound to, is resistant to oxidation with ΔE_{L_ox} around +2.5 eV. The same holds for dma with $\Delta E_{L\_ox} \approx$ +1.2 eV, except for $Mg(NMe_2)_2$ that can dissociate its ligand to the O in the As_2O_3 substrate with ΔE_{L_ox} a little below 0 eV. On the contrary, the methyl group is always susceptible to oxidation with exothermic ΔE_{L_ox} for all metal precursors selected.

Figure 6. Computed energetics for ligand oxidation at the surface, L = $[N(Me)_2]^-$, $[Me]^-$, $[Cl]^-$, and As_2O_3 reduction according to: $||As\text{-}O|| + \frac{1}{n} ML_{n\,(g)} \rightarrow M_{\frac{1}{n}}O_{\frac{1}{2}\,(bulk)} + ||O\text{-}L + ||As\text{-}As||$ for M = Mg(II), Al(III), Ti(IV), Zr(IV), Hf(IV), Ta(V). Lines are to guide the eye.

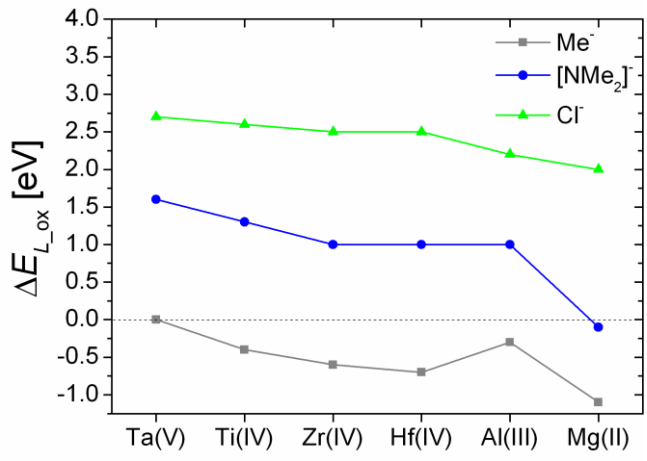

The second factor affecting clean-up is substrate chemistry. If a ligand is susceptible to decomposition, specific sites on the surface can activate some bonds of the ligand and this can trigger secondary surface reactions that result in clean-up. C-H and N-C bonds of the dma ligand can be activated even at relatively low temperature as discussed in previous sections. It has been shown that especially mixed nucleophilic-electrophilic character of the surface sites, *e.g.* the zwitterionic character of silicon, affects reactivity and transformations of alkylamides [29]. Such reactivity of alkylamides is confirmed by experimental observation of formation of Si-H bonds accompanied by the formation of Si-C bonds

620 (leading to incorporation of carbon into the deposited film). Low temperature production of methane has
621 also been observed, which is evidence for N-C reactivity when depositing oxide films on bare Si or
622 hydrogen terminated Si substrates. In our calculations, we see similar behaviour of the alkylamide
623 ligand on the relatively weakly amphoteric As_2O_3 substrate. On this oxide substrate H is removed from
624 the ligand as a proton and formation of O-H bonds is plausible. In this process clean-up is achieved, as
625 well as producing additional reactive sites (OH) for ALD, but at the same time *M*-C bonds are formed.
626 This is because proton elimination causes changes in electronic density on alkylamide carbons: the CH_2
627 fragment becomes Lewis basic and this promotes *M*-C formation (**B**), or the CH_3 fragment attracts the
628 charge, and CH_3^- detachment is promoted, resulting also in *M*-C formation (**J**). Some of these reactions
629 may be more strongly favoured on the mixture of more electropositive Ga^{3+} and In^{3+} sites of the real III-
630 V surfaces or even the M^{n+} sites of the growing film, where bonds tend to be more ionic rather than
631 covalent. Based on this we can conclude that the above-mentioned mechanisms account for the
632 reactivity and behaviour of metal alkylamides and can be expected on various substrates featuring Lewis
633 acid/base sites.

634 An important aspect is whether these processes occur during homodeposition (*i.e.* during the later stages
635 of growth of *e.g.* HfO_2 onto HfO_2) and give a CVD component to standard ALD. Clearly during
636 homodeposition there is no extra driving force from M_2O_n formation. On the other hand, decomposition
637 reactions may be more favoured on the growing film owing to its pronounced nucleophilic-electrophilic
638 or Lewis acid/base character, as mentioned above. According to our computations, processes yielding
639 **B**-**K** are energetically uphill from formation of intermediate **A** onwards. However the formation of **B**
640 and **J** are only +0.5 eV and +0.8 eV uphill respectively at 0 K for the clean-up process on the As_2O_3
641 substrate and can be expected at elevated temperatures. This finding is supported by experimental
642 observation of increased efficiency of clean-up with increased temperature. Another aspect is simple
643 consideration of the strength of the As-O bond and, using the example of HfO_2, the Hf-O bond. Clearly
644 the Hf-O bond, once it is formed, is much stronger and less reactive, which does not favour subsequent

645 CVD reactions. An explicit investigation of CVD reactions on the HfO_2 surface is necessary to fairly
646 judge the importance of the CVD contribution in case of alkylamide ALD, but is beyond the scope of
647 this paper.

648 4. Conclusion

649 We successfully apply our model for clean-up to explain differences in the performance of various
650 classes of precursor chemicals in removing native oxide from III-V substrates. Building on the example
651 of TMA, we identify two separate factors governing the clean-up effect: formation of the metal oxide as
652 the primary driving force and affinity of the precursor ligand to the III-V oxide substrate as the ancillary
653 force. That allows an efficient description of interactions of the various precursor ligands with an
654 oxidised III-V substrate, and of the associated multi-step chemical processes that lead to formation of
655 the clean-up products. We map out reaction sequences for the alkylamide ligand that lead plausibly to
656 products that are detected experimentally (aziridine, ethylene, MMI, HCN, methane). Through this
657 approach, a set of general reactions is generated and comparison is made between several different
658 precursors, including metal alkylamides $Mg[N(CH_3)_2]_2$, $Al[N(CH_3)_2]_3$, $Ti[N(CH_3)_2]_4$, $Zr[N(CH_3)_2]_4$,
659 $Hf[N(CH_3)_2]_4$, $Ta[N(CH_3)_2]_5$; metal methyls: $Mg(CH_3)_2$, $Al(CH_3)_3$, $Ti(CH_3)_4$, $Zr(CH_3)_4$, $Hf(CH_3)_4$,
660 $Ta(CH_3)_5$; and metal chlorides: $MgCl_2$, $AlCl_3$, $TiCl_4$, $ZrCl_4$, $HfCl_4$, $TaCl_5$. We can therefore predict the
661 best reagent for achieving the clean-up effect.
662 We predict that the investigated methyl precursors are the best reagents for deposition of dielectrics and
663 performing clean-up. Unfortunately, most of them are very unstable compounds. Clean-up is most
664 effective when depositing MgO, as Mg^{2+} works as the most effective scavenger of O^{2-}. Clean-up with
665 metal chlorides seems to have a fundamentally different mechanism, probably involving removal of the
666 O from the native oxide film and passivation with Cl groups.
667 The first principles study shows that clean-up with metal alkylamides has a similar mechanism to clean-
668 up with metal methyls as regards the scavenging of oxygen from weak As, Ga and In oxides. Arising
669 from this, ligand exchange can in principle lead to a clean-up product: tris(dimethylamino)arsine.

However steric hindrance and the bulky character of the alkylamide ligand are rate limiting factors, which in this case are very pronounced and suggest that this particular reaction will not proceed.

Our study also shows the difference in mechanism underlying the consumption of III-V oxides with alkylamido precursors from the one taking place with TMA. In the case of the alkylamide ligand, thermal decomposition rather than migration of the entire ligand on the oxide surface is dominant, taking into account the bulky character of the ligand and its known reactivity in contact with a semiconductor or metallic surface. Clean-up of the reducible As oxide substrate is therefore enhanced by secondary decomposition surface reactions, not by oxidation of the entire alkylamide. The H elimination process that forms hydroxyl groups and As-C bound species (**B**) is exothermic or neutral at 0 K and kinetically demanding. The migration of these decomposition intermediates from an As site to an O site (**C**) and direct reduction of the substrate is only slightly endothermic. Successive dehydrogenation though becomes progressively less favored. Instead, the first H elimination may be followed by another plausible reaction – N-C bond scission (**J**), which can lead to low temperature methane production, albeit without the clean-up effect. Thermal activation is needed for formation and desorption of products that arise from these decomposition structures: most likely N-methylmethyleneimine and aziridine, possibly along with methane, ethylene and dinitrogen. A specific requirement of the substrate is that it contain both Lewis acid and Lewis base sites, which can activate secondary surface reactions of ligands that are susceptible to decomposition, like the dimethylamido group. These redox processes do lead to the reduction of arsenic oxides to metallic arsenic, which in turn can reduce gallium and indium oxides to pure III-V material. Some of the reactions that we have presented therefore account for the clean-up effect, but they occur in parallel with reactions that do not achieve clean-up.

More generally we show that organometallic reagents react readily with substrates featuring less electropositive metals. In presence of metals like Si, As, Ga and In, a reactive polar metal-organic ligand bond, *e.g.* Al-C, is broken and formation of more covalent bond, *e.g.* As-C, is favoured. These reactions

might be possible during homodeposition and can thereby give a CVD component to standard ALD, as is well-documented for alkylamides. The mechanisms described here are in line with observations on Si surfaces as well. The same mechanisms can therefore be expected on other substrates, such as oxides and nitrides, that show a mix of Lewis acid/base sites.

ASSOCIATED CONTENT

Supporting Information Available: lattice parameters and space groups, along with *k*-point sampling for optimised bulk structures; geometrical parameters for optimised gaseous molecules; additional list of possible clean-up *intermediates* that are formed during ALD III-V substrate exposure to alkylamide metal precursors – energetics for the interaction of dma ligand with the substrate (ΔE_L); surface models showing products of the dissociative adsorption of $Hf[N(CH_3)_2]_4$ precursor; reaction profile for dissociative adsorption of $Hf[N(CH_3)_2]_4$ precursor; energetics for ligand exchange between precursor metal centre and bulk III-V oxide: As_2O_3, As_2O_5, Ga_2O_3 and In_2O_3 for L = $[Me]^-$; $[Cl]^-$.

This material is available free of charge via the Internet at http://pubs.acs.org.

AUTHOR INFORMATION

Corresponding author

**E-mail address*: simon.elliott@tyndall.ie.

Notes

The authors declare no competing financial interest.

718 ACKNOWLEDGMENT

719 This work was funded by Science Foundation Ireland under grant no. 07/SRC/I1172 ("FORME",
720 www.tyndall.ie/forme). The authors wish to acknowledge the SFI/HEA Irish Centre for High-End
721 Computing (ICHEC) for the provision of computational facilities and support.

722

723 REFERENCES

724 1. Miikkulainen, V.; Leskela, M.; Ritala, M.; Puurunen, R. L., Crystallinity of inorganic films
725 grown by atomic layer deposition: Overview and general trends. *Journal of Applied Physics* **2013,** *113*
726 (2), 021301-101.
727 2. Huang, M. L.; Chang, Y. C.; Chang, C. H.; Lee, Y. J.; Chang, P.; Kwo, J.; Wu, T. B.; Hong, M.,
728 Surface passivation of III-V compound semiconductors using atomic-layer-deposition-grown Al_2O_3.
729 *Applied Physics Letters* **2005,** *87* (25), 252104-3.
730 3. (a) Chang, C. H.; Chiou, Y. K.; Chang, Y. C.; Lee, K. Y.; Lin, T. D.; Wu, T. B.; Hong, M.;
731 Kwo, J., Interfacial self-cleaning in atomic layer deposition of HfO_2 gate dielectric on $In_{0.15}Ga_{0.85}As$.
732 *Applied Physics Letters* **2006,** *89* (24), 242911-3; (b) Delabie, A.; Brunco, D. P.; Conard, T.; Favia, P.;
733 Bender, H.; Franquet, A.; Sioncke, S.; Vandervorst, W.; Van Elshocht, S.; Heyns, M.; Meuris, M.; Kim,
734 E.; McIntyre, P. C.; Saraswat, K. C.; LeBeau, J. M.; Cagnon, J.; Stemmer, S.; Tsai, W., Atomic Layer
735 Deposition of Hafnium Oxide on Ge and GaAs Substrates: Precursors and Surface Preparation. *Journal*
736 *of The Electrochemical Society* **2008,** *155* (12), H937-H944.
737 4. (a) Granados-Alpizar, B.; Muscat, A. J., Surface reactions of $TiCl_4$ and $Al(CH_3)_3$ on GaAs(100)
738 during the first half-cycle of atomic layer deposition. *Surface Science* **2011,** *605* (13-14), 1243-1248; (b)
739 Gougousi, T.; Lacis, J. W., Native oxide consumption during the atomic layer deposition of TiO_2 films
740 on GaAs (100) surfaces. *Thin Solid Films* **2010,** *518* (8), 2006-2009.

741 5. Gougousi, T.; Ye, L., Interface Between Atomic Layer Deposition Ta_2O_5 Films and GaAs(100)
742 Surfaces. *The Journal of Physical Chemistry C* **2012,** *116* (16), 8924-8931.
743 6. (a) Tallarida, M.; Adelmann, C.; Delabie, A.; Van Elshocht, S.; Caymax, M.; Schmeisser, D.,
744 Surface chemistry and Fermi level movement during the self-cleaning of GaAs by trimethyl-aluminum.
745 *Applied Physics Letters* **2011,** *99* (4), 042906; (b) Lin, L.; Robertson, J., Defect states at III-V
746 semiconductor oxide interfaces. *Appl. Phys. Lett.* **2011,** *98* (8), 082903.
747 7. (a) O'Mahony, A.; Monaghan, S.; Chiodo, R.; Povey, I.; Cherkaoui, K.; Nagle, R.; O'Connor, E.;
748 Long, R.; Djara, V.; O'Connell, D.; Crupi, F.; Pemble, M.; Hurley, P. K., Structural and Electrical
749 Analysis of Thin Interface Control Layers of MgO or Al_2O_3 Deposited by Atomic Layer Deposition and
750 Incorporated at the High-k/III-V Interface of $MO_2/In_xGa_{1-x}As$ (M = Hf|Zr, x = 0|0.53) Gate Stacks. *ECS*
751 *Transactions* **2010,** *33* (2), 69-82; (b) O'Mahony, A.; Monaghan, S.; Provenzano, G.; Povey, I. M.;
752 Nolan, M. G.; O'Connor, E.; Cherkaoui, K.; Newcomb, S. B.; Crupi, F.; Hurley, P. K.; Pemble, M. E.,
753 Structural and electrical analysis of the atomic layer deposition of HfO_2/n-$In_{0.53}Ga_{0.47}As$ capacitors with
754 and without an Al_2O_3 interface control layer. *Applied Physics Letters* **2010,** *97* (5), 052904-3; (c)
755 O'Connor, E.; Brennan, B.; Djara, V.; Cherkaoui, K.; Monaghan, S.; Newcomb, S. B.; Contreras, R.;
756 Milojevic, M.; Hughes, G.; Pemble, M. E.; Wallace, R. M.; Hurley, P. K., A systematic study of
757 $(NH_4)_2S$ passivation (22%, 10%, 5%, or 1%) on the interface properties of the $Al_2O_3/In_{0.53}Ga_{0.47}As$/InP
758 system for n-type and p-type $In_{0.53}Ga_{0.47}As$ epitaxial layers. *Journal of Applied Physics* **2011,** *109* (2),
759 024101-10; (d) Monaghan, S.; O'Mahony, A.; Cherkaoui, K.; O'Connor, E.; Povey, I. M.; Nolan, M. G.;
760 O'Connell, D.; Pemble, M. E.; Hurley, P. K.; Provenzano, G.; Crupi, F.; Newcomb, S. B. In *Electrical*
761 *analysis of three-stage passivated $In_{0.53}Ga_{0.47}As$ capacitors with varying HfO_2 thicknesses and*
762 *incorporating an Al_2O_3 interface control layer*, AVS: 2011; pp 01A807-8.
763 8. Hinkle, C. L.; Sonnet, A. M.; Vogel, E. M.; McDonnell, S.; Hughes, G. J.; Milojevic, M.; Lee,
764 B.; Aguirre-Tostado, F. S.; Choi, K. J.; Kim, H. C.; Kim, J.; Wallace, R. M., GaAs interfacial self-
765 cleaning by atomic layer deposition. *Applied Physics Letters* **2008,** *92* (7), 071901-3.

9. Gougousi, T.; Hackley, J. C.; Demaree, J. D.; Lacis, J. W., Growth and Interface Evolution of HfO_2 Films on GaAs(100) Surfaces. *Journal of The Electrochemical Society* **2010,** *157* (5), H551-H556.

10. Frank, M. M.; Wilk, G. D.; Starodub, D.; Gustafsson, T.; Garfunkel, E.; Chabal, Y. J.; Grazul, J.; Muller, D. A., HfO_2 and Al_2O_3 gate dielectrics on GaAs grown by atomic layer deposition. *Applied Physics Letters* **2005,** *86* (15), 152904-3.

11. Milojevic, M.; Aguirre-Tostado, F. S.; Hinkle, C. L.; Kim, H. C.; Vogel, E. M.; Kim, J.; Wallace, R. M., Half-cycle atomic layer deposition reaction studies of Al_2O_3 on $In_{0.2}Ga_{0.8}As$ (100) surfaces. *Applied Physics Letters* **2008,** *93* (20), 202902-3.

12. Elliott, S. D., Atomic-scale simulation of ALD chemistry. *Semiconductor Science and Technology* **2012,** *27* (7), 074008.

13. Hegde, G.; Klimeck, G.; Strachan, A., Role of surface orientation on atomic layer deposited Al_2O_3/GaAs interface structure and Fermi level pinning: A density functional theory study. *Applied Physics Letters* **2011,** *99* (9), 093508-3.

14. Klejna, S.; Elliott, S. D., First-Principles Modeling of the "Clean-Up" of Native Oxides during Atomic Layer Deposition onto III–V Substrates. *The Journal of Physical Chemistry C* **2012,** *116* (1), 643-654.

15. Kresse, G.; Furthmüller, J., Efficient iterative schemes for ab initio total-energy calculations using a plane-wave basis set. *Physical Review B* **1996,** *54* (16), 11169.

16. Perdew, J. P.; Chevary, J. A.; Vosko, S. H.; Jackson, K. A.; Pederson, M. R.; Singh, D. J.; Fiolhais, C., Atoms, molecules, solids, and surfaces: Applications of the generalized gradient approximation for exchange and correlation. *Physical Review B* **1992,** *46* (11), 6671.

17. (a) Vanderbilt, D., Soft self-consistent pseudopotentials in a generalized eigenvalue formalism. *Physical Review B* **1990,** *41* (11), 7892; (b) Kresse, G.; Hafner, J., Norm-conserving and ultrasoft pseudopotentials for first-row and transition elements. *Journal of Physics: Condensed Matter* **1994,** *6* (40), 8245.

18. Wyckoff, R. W. G., Crystal Structures. *Crystal Structures* **Wiley Interscience, New York, 1963**.

19. Ballirano, P.; Maras, A. Z., Refinment of the crystal structure of arsenolite, As_2O_3. *Kristallogr.-New Cryst. Struct.* **2002,** *217*, 177-178.

20. Henkelman, G.; Arnaldsson, A.; Jónsson, H., A fast and robust algorithm for Bader decomposition of charge density. *Computational Materials Science* **2006,** *36* (3), 354-360.

21. Henkelman, G.; Uberuaga, B. P.; Jonsson, H., A climbing image nudged elastic band method for finding saddle points and minimum energy paths. *The Journal of Chemical Physics* **2000,** *113* (22), 9901-9904.

22. (a) Murray, C.; Elliott, S. D., Density Functional Theory Predictions of the Composition of Atomic Layer Deposition-Grown Ternary Oxides. *ACS Applied Materials & Interfaces* **2013,** *5* (9), 3704-3715; (b) Elliott, S. D., Improving ALD growth rate via ligand basicity: Quantum chemical calculations on lanthanum precursors. *Surface and Coatings Technology* **2007,** *201* (22–23), 9076-9081.

23. Suri, R.; Lichtenwalner, D. J.; Misra, V., Interfacial self cleaning during atomic layer deposition and annealing of HfO_2 films on native (100)-GaAs substrates. *Applied Physics Letters* **2010,** *96* (11), 112905-3.

24. Lamagna, L.; Wiemer, C.; Perego, M.; Spiga, S.; Rodríguez, J.; Santiago Coll, D.; Grillo, M. E.; Klejna, S.; Elliott, S. D., Mechanisms for Substrate-Enhanced Growth during the Early Stages of Atomic Layer Deposition of Alumina onto Silicon Nitride Surfaces. *Chemistry of Materials* **2012,** *24* (6), 1080-1090.

25. (a) Marx, D.; Asahi, H.; Liu, X. F.; Higashiwaki, M.; Villaflor, A. B.; Miki, K.; Yamamoto, K.; Gonda, S.; Shimomura, S.; Hiyamizu, S., Low temperature etching of GaAs substrates and improved morphology of GaAs grown by metalorganic molecular beam epitaxy using trisdimethylaminoarsenic and triethylgallium. *Journal of Crystal Growth* **1995,** *150, Part 1* (0), 551-556; (b) Salim, S.; Ping Lu, J.; Jensen, K. F.; Bohling, D. A., Surface reactions of dimethylaminoarsine during MOMBE of GaAs. *Journal of Crystal Growth* **1992,** *124* (1–4), 16-22; (c) Shi, B.; Tu, C., A kinetic model for

817 tris(dimethylamino) arsine decomposition on GaAs(100) surfaces. *Journal of Electronic Materials*
818 **1999,** *28* (1), 43-49.
819 26. Puurunen, R. L., Formation of Metal Oxide Particles in Atomic Layer Deposition During the
820 Chemisorption of Metal Chlorides: A Review. *Chemical Vapor Deposition* **2005,** *11* (2), 79-90.
821 27. Kim, T.; Zaera, F., Surface Chemistry of Pentakis(dimethylamido)tantalum on Ta Surfaces. *The*
822 *Journal of Physical Chemistry C* **2011,** *115* (16), 8240-8247.
823 28. Li, K.; Li, S.; Li, N.; Dixon, D. A.; Klein, T. M., Tetrakis(dimethylamido)hafnium Adsorption
824 and Reaction on Hydrogen Terminated Si(100) Surfaces. *The Journal of Physical Chemistry C* **2010,**
825 *114* (33), 14061-14075.
826 29. (a) Rodríguez-Reyes, J. C., Mechanisms of adsorption and decomposition of metal alkylamide
827 precursors for ultrathin film growth. *J. Appl. Phys.* **2008,** *104* (8), 084907; (b) Rodríguez-Reyes, J. C.
828 F.; Teplyakov, A. V., Chemisorption of Tetrakis(dimethylamido)titanium on Si(100)-2 × 1: C−H and
829 C−N Bond Reactivity Leading to Low-Temperature Decomposition Pathways. *The Journal of Physical*
830 *Chemistry C* **2008,** *112* (26), 9695-9705.
831 30. (a) Bradley, D. C.; Chisholm, M. H., Transition-metal dialkylamides and disilylamides.
832 *Accounts of Chemical Research* **1976,** *9* (7), 273-280; (b) Salim, S.; Lim, C. K.; Jensen, K. F., Gas-
833 Phase Decomposition Reactions of Tris(dimethylamino)phosphine, -Arsine, and -Stibine Reagents.
834 *Chemistry of Materials* **1995,** *7* (3), 507-516.
835 31. Ando, T., Ultimate Scaling of High-κ Gate Dielectrics: Higher-κ or Interfacial Layer
836 Scavenging? *Materials* **2012,** *5* (3), 478-500.
837
838
839

840 TABLE OF CONTENTS (TOC)

841 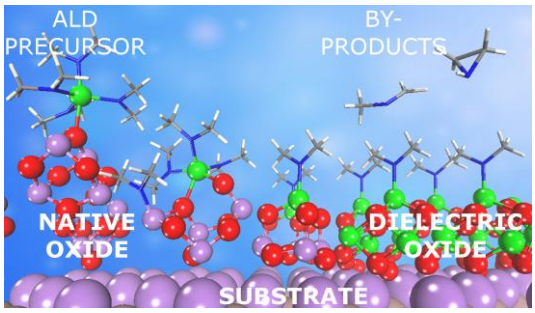

842 Deleterious native oxides of semiconductor substrate are transformed into dielectric oxide when atomic
843 layer deposition technique (ALD) with the appropriate precursor chemical is used during transistor
844 fabrication.

845